Effect of charge transfer to the conduction band within a single-impurity model on the Ni 2p core-level line shapes of Ni compounds

A. E. Bocquet, T. Mizokawa, and A. Fujimori
Department of Physics, University of Tokyo, Bunkyo-ku, Tokyo 113, Japan

M. Matoba and S. Anzai
Faculty of Science and Technology, Keio University, Hiyoshi, Yokohama 223, Japan
(Received 26 May 1995)

We have extended the single-impurity cluster model to include the effects of charge transfer to the conduction band. It is found that these effects can have a considerable influence on the line shapes of core-level spectra of small-gap transition-metal compounds. Using a few additional, well-defined parameters to describe the interactions between the local cluster and the conduction band, and retaining the original intracluster parameters from previous single-impurity models, we find an improved agreement for the Ni 2p spectrum of NiS. The asymmetric line shape is well reproduced, keeping the correct satellite to main peak ratio, which is not possible using the three-peak structure of previous models. The new model is less successful in explaining effects beyond standard single-impurity models in more ionic compounds, such as the double-peak stucture of the main line of the core-level spectrum of NiO, where the interactions between the metal d site and the conduction band are expected to play a lesser role.

I. INTRODUCTION

In recent years, the use of model Hamiltonians based on a single-impurity model in Anderson impurity[1,2] or cluster calculations[3–6] of core-level spectra has been largely successful in identifying the important parameters for the electronic structure of transition-metal (TM) compounds. For example, analysis of the line shapes of the metal 2p spectra of the late 3d TM compounds using a cluster-type configuration-interaction (CI) model reveals systematic trends in the on site d-d Coulomb interaction energy U, the charge-transfer energy Δ, and the metal-to-ligand transfer integral T_σ for a wide range of compounds.[6] In a single-impurity model, we consider only a single TM ion surrounded by ligand atoms in a cluster. For the late TM compounds, the lowest-energy final state will often be a screened state of the form $\underline{c}3d^{n+1}\underline{L}$, with the satellite structure arising from $\underline{c}3d^n$ or $\underline{c}3d^{n+2}\underline{L}^2$ states,[6] where $\underline{c}$ represents a core hole and $\underline{L}$ refers to a hole in the ligand band. The justification for the use of a single-impurity approach is that the electronic structures of the TM compounds are dominated by local interactions.

However, a number of structures appear in the core-level spectra that cannot be explained by a simple single-impurity model. These include the asymmetric line shape of the 2p core levels of many metallic or semiconducting TM compounds, such as NiS (Ref. 7) and FeS_2.[6] Recently, additional structures in the metal 2p core-level line shapes of CuO (Ref. 8) and NiO (Ref. 9) have been reexamined using multiple-impurity models,[8–13] where the impurity unit is extended from a single cluster to include more than one TM ion. By taking into account nonlocal screening effects from neighboring TM sites, such models have been successful in explaining the large width of the CuO Cu 2p main line[8] and the doubly peaked structure of the NiO Ni 2p main line.[9] These additional structures arise from energetically different screening channels in the final state, where the main peak is now due to states screened either by a ligand electron of the local cluster or by a ligand electron from a neighboring cluster.

In order to explain the asymmetric line shape of the 2p core levels of the metallic or semiconducting TM chalcogenides, one may introduce the effect of charge transfer to an empty conduction band within the framework of a single-impurity model. Here, we retain only a single TM ion cluster, but allow charge transfer between the TM site and the ligand sites and the TM site and the conduction band. For most 3d TM compounds, the lowest-lying conduction band is simply the upper Hubbard band and the orbitals making up this conduction-band level will consist of empty 3d orbitals from neighboring d-electron sites. For compounds with a small band gap, such as NiS, which undergoes a metal-insulator transition as a function of pressure or temperature,[14] such charge-transfer effects are expected to play an important role in the electronic structure. This model provides a good starting point to describe the electronic structure of compounds in which the empty states have considerable mixed ligand p character due to strong covalency, and so are hybridized with the metal d orbitals. The inclusion of states where electrons have been transferred to the conduction band has been shown to be important even for insulating compounds such as Cu_2O, where the d-electron number from *ab initio* calculations,[15] 9.30, is found to be somewhat less than 10. Karlsson, Gunnarsson, and Jepsen[16] have shown, using an Anderson impurity calculation, that the inclusion of states where an electron has hopped into the conduction band has important consequences for the interpretation of the core-level x-ray photoemission

(XPS) spectra of Cu_2O, CuO, and $NaCuO_2$.

In this work, we introduce a configuration-interaction cluster model, where charge transfer to the conduction-band level is included within a single-impurity framework. These effects can be described by a few additional, well-defined, parameters. The model retains the simplicity and generality of the single-cluster approach, while taking into account nonlocal effects in an approximate way, and so has the potential to be generally applied. Using this approach, we have reinterpreted the Ni $2p$ core-level spectrum of NiS, which shows a considerably asymmetric main peak line shape. By retaining the original parameters U, Δ, and T_σ describing the local intracluster interactions from previous single-impurity models,[6,17,18] and introducing the effects of charge transfer to the conduction band, we can reproduce the asymmetry of the main peak well, while keeping the correct satellite to main peak ratio, which cannot be fitted using the three-peak structure of a simple cluster model. We also calculate the spectrum for NiO using this model and show that this model and show that the origin of the extra structure in the main peak is different from that found by a multiple-impurity approach.

The organization of this paper is as follows. First, the Hamiltonian and model parameters used for the calculation of the spectra will be described. The model is then used to reinterpret the Ni $2p$ core-level XPS spectrum of NiS. Various predictions on the electronic structure of this compound are also discussed. Subsequently, results for NiO found by this approach are compared to results obtained from a multiple-impurity model.

II. DESCRIPTION OF THE MODEL

A. The cluster model including a conduction band

We use to describe the spectra a single-impurity cluster model consisting of a central TM ion surrounded by ligand atoms and including the presence of a conduction band. In the cluster approximation, the bandwidths of the valence and conduction bands are collapsed to zero, and they are considered as single energy levels for simplicity. We start from the limit of weak hybridization. Within the CI picture, we consider the TM atom to be in an ionic d^n configuration and the valence and conduction bands to be completely filled and empty, respectively. The energy of this ionic state $|d^n\rangle$, averaged over all mulitplet terms, is given by

$$E(d^n)=E_0+n\varepsilon_d^0+\tfrac{1}{2}n(n-1)U \ , \tag{1}$$

where E_0 is the energy of the host structure including the filled valence and empty conduction bands, ε_d^0 is the bare d-electron energy including the Madelung potential at the cation site, and U is the average Coulomb repulsion energy. Charge transfer between the d-electron site and the valence- and conduction-band levels produces configurations such as $d^{n+1}\underline{L}$, $d^{n+2}\underline{L}^2,\ldots,d^{n-1}C$, $d^{n-2}C^2,\ldots,d^n\underline{L}C$, $d^n\underline{L}^2C^2,\ldots,d^{n+1}\underline{L}^2C$, $d^{n-1}\underline{L}C^2,\ldots$, etc., where $\underline{L}$ denotes a hole in a ligand p orbital and C denotes an electron in the conduction band.

The energy required for charge transfer from the filled valence band to the d-electron site, Δ, is defined from (1) as in previous models as

$$\Delta\equiv E(d^{n+1}\underline{L})-E(d^n)\equiv\varepsilon_d^0-\varepsilon_V+nU \ , \tag{2}$$

where ε_V is the energy of the valence-band level. Similarly, we can define a charge-transfer energy to the empty conduction band,[19] Δ^*, as the energy required to transfer an electron away from the d-electron site, $d^n\rightarrow d^{n-1}C$:

$$\Delta^*\equiv E(d^{n-1}C)-E(d^n)\equiv\varepsilon_c-\varepsilon_d^0-(n-1)U \ , \tag{3}$$

where ε_c is the conduction-band level.

The wave function for the formally d^n ground state spanned by the above configurations can be written as

$$\psi_g=\sum_{l,m}a_{l,m}|d^{(n+l-m)}\underline{L}^lC^m\rangle \ , \tag{4}$$

where n is the number of d electrons, and the right-hand side is summed over the number of ligand holes $l=0,1,2,\ldots,10-n-m$, and the number of electrons transferred to the conduction band $m=0,1,2,\ldots,n+l$. The bare ionic state d^n occurs for $l,m=0$. Here, crystal-field effects and the d-d exchange interaction are accounted for by extending the basis set to distinguish between each individual orbital and spin state. Thus, the charge-transfer basis states of (4) can be written more generally as

$$|d^n\rangle \ , \tag{5}$$

$$|d^{n+1}\underline{L}\rangle=\frac{1}{\sqrt{10-n}}\sum_\mu d_\mu^\dagger p_\mu|d^n\rangle \ , \tag{6}$$

$$|d^{n+2}\underline{L}^2\rangle=\left[\frac{2}{(10-n)(9-n)}\right]^{1/2}\sum_{\substack{\mu,\mu'\\ \mu\neq\mu'}}d_\mu^\dagger d_{\mu'}^\dagger p_\mu p_{\mu'}|d^n\rangle \ , \tag{7}$$

$$|d^{n-1}C\rangle=\frac{1}{\sqrt{n}}\sum_\nu d_\nu c_\nu^\dagger|d^n\rangle \ , \tag{8}$$

$$|d^{n-2}C^2\rangle=\left[\frac{2}{n(n-1)}\right]^{1/2}\sum_{\substack{\nu,\nu'\\ \nu\neq\nu'}}d_\nu d_{\nu'}c_\nu^\dagger c_{\nu'}^\dagger|d^n\rangle \ , \tag{9}$$

$$|d^n\underline{L}C\rangle=\frac{1}{\sqrt{n(10-n)}}\sum_{\mu,\nu}d_\mu^\dagger d_\nu p_\mu c_\nu^\dagger|d^n\rangle \ , \tag{10}$$

etc., where $d^\dagger$ and d are the creation and annihilation operators for d electrons, p is the annihilation operator for the ligand p electrons, and $c^\dagger$ is the creation operator for conduction-band electrons. Here, μ and ν are combined orbital and spin indices indicating the unfilled and filled electron levels, respectively, for the configuration before the charge transfer took place. For example, for a high spin d^8 compound, the orbitals for (6) and (8) labeled by μ are the unoccupied $(x^2-y^2)\downarrow$ and $(3z^2-r^2)\downarrow$ levels, while those labeled by ν are the remaining occupied eight levels. The basis states are approximated by single Slater determinants and all core-hole–d-electron multiplet effects have been neglected. For a system with

formally n d electrons, the ligand orbitals can transfer up to 10-n electrons to the TM site, while up to n electrons can be transferred to the conduction band. Charge-transfer states can mix within ionic states if they preserve the same symmetry. If the conduction band is considered to be the upper Hubbard band formed by empty $3d$ orbitals on antiferromagnetically ordered nearest-neighboring TM sites, for a structure of ideal cubic symmetry, only 10-n electrons with the correct orbital symmetry can be transferred from the d site to the conduction-band orbitals for each nearest-neighbor site. Configurations of the type $d^n\underline{L}C$ will also involve states where an electron is effectively transferred from a ligand orbital to the conduction band via the central TM site. This means that even for systems with mostly filled $3d$ orbitals, the number of configurations increases rapidly with each possible charge-transfer process. Thus, in order to reduce the size of the calculations, the basis set is truncated after up to six charge-transfer processes (e.g., at configurations of the type $d^{n+6}\underline{L}^6, \ldots, d^{n+2}\underline{L}^4C^2$, $d^n\underline{L}^3C^3$, $d^{n-2}\underline{L}^2C^4, \ldots, d^{n-6}C^6$, where the total number of d-electrons $N=n+l-m$ is $0\le N\le 10$).

The Coulomb-exchange-interaction energy for each configuration $\varepsilon(d^{n+l-m}\underline{L}^lC^m)$ is expressed in terms of the Kanamori parameters[6,20] u, u',and j, and calculated using the Racah parameters A, B, and C in a manner identical to that of earlier models.[6] The crystal-field splitting, $10Dq$, which is expected to be in the order of 0.5 eV was neglected for simplicity.[6] The diagonal Hamiltonian matrix elements for the ground-state basis states can be expressed in terms of the parameters Δ, Δ^*, and U. These are given successively by

$$
\begin{aligned}
&\langle d^n|H|d^n\rangle = 0 \text{ (reference)} ,\\
&\langle d^{n+1}\underline{L}|H|d^{n+1}\underline{L}\rangle = \varepsilon(d^{n+1}\underline{L}) - \varepsilon(d^n) + \Delta ,\\
&\langle d^{n+2}\underline{L}^2|H|d^{n+2}\underline{L}^2\rangle = \varepsilon(d^{n+2}\underline{L}^2) - \varepsilon(d^n) + 2\Delta + U, \ldots ,\\
&\langle d^{n-1}C|H|d^{n-1}C\rangle = \varepsilon(d^{n-1}C) - \varepsilon(d^n) + \Delta^* ,\\
&\langle d^{n-2}C^2|H|d^{n-2}C^2\rangle \\
&\qquad = \varepsilon(d^{n-2}C^2) - \varepsilon(d^n) + 2\Delta^* + U, \ldots ,\\
&\langle d^n\underline{L}C|H|d^n\underline{L}C\rangle = \varepsilon(d^n\underline{L}C) - \varepsilon(d^n) + \Delta + \Delta^* - U ,\\
&\langle d^n\underline{L}^2C^2|H|d^n\underline{L}^2C^2\rangle \\
&\qquad = \varepsilon(d^n\underline{L}^2C^2) - \varepsilon(d^n) + 2(\Delta + \Delta^* - U), \ldots ,\\
&\langle d^{n+l-m}\underline{L}^lC^m|H|d^{n+l-m}\underline{L}^lC^m\rangle \\
&\quad = \varepsilon(d^{n+l-m}\underline{L}^lC^m) - \varepsilon(d^n) \\
&\qquad + m(\Delta + \Delta^* - U) + (l-m)\Delta \\
&\qquad + \tfrac{1}{2}(l-m)(l-m-1)U \quad \text{for } l \ge m ,\\
&\langle d^{n+l-m}\underline{L}^lC^m|H|d^{n+l-m}\underline{L}^lC^m\rangle \\
&\quad = \varepsilon(d^{n+l-m}\underline{L}^lC^m) - \varepsilon(d^n) \\
&\qquad + l(\Delta + \Delta^* - U) + (m-l)\Delta^* \\
&\qquad + \tfrac{1}{2}(m-l)(m-l-1)U \quad \text{for } m \ge l .
\end{aligned}
\tag{11}
$$

Here, the energy of the $|d^n\underline{L}C\rangle$ state is simply that required to transfer an electron from the valence band to the conduction band and is equal to the magnitude of the band gap, $\Delta+\Delta^*-U$. It should be noted that the parameters Δ, Δ^*, and U are all defined with respect to the center of gravity of the multiplet of each configuration. Parameters Δ_{eff}, Δ^*_{eff}, and U_{eff} can also be defined with respect to the lowest multiplet level.[17–19]

B. Application to the photoemission spectra of TM compounds

The model presents us with a number of possible scenarios for the conduction band and the magnitude of Δ^*. For most $3d$ TM compounds, such as NiS and NiO, the lowest-lying conduction-band level, which defines the magnitude of Δ^*, can be either the upper Hubbard band formed by empty $3d$ orbitals on neighboring TM sites (scenario 1), or the wide conduction band consisting of the TM metal $4sp$ states (scenario 2). Both these empty states orbitals can be strongly hybridized with the ligand orbitals and have a significant p character. Scenario 1 includes multiple TM ions and simulates in an approximate way the effects of additional TM sites within the lattice, with Δ^* being exactly equal to U, the energy required to transfer an electron from the lower to the upper Hubbard bands. For scenario 2, Δ^* will be somewhat larger than U, with the metal $4sp$ levels lying some 5 eV above the empty $3d$ levels, as found from inverse photoemission spectroscopy.[21] In this work, we will mainly consider scenario 1, as scenario 2 has been found to show little difference from the simple-cluster model as we will show later. In scenario 1, the band gap $\Delta+\Delta^*-U$ will be exactly equal to the charge-transfer energy Δ, and the configurations $d^{n+1}\underline{L}$ and $d^n\underline{L}C$ will be degenerate in the unhybridized ground state. Figure 1 shows the many-electron total-energy scheme for the unhybridized ground state in this case, for the neutral (n-electron), electron-addition ($n+1$ electron), and electron-removal ($n-1$ electron) states.

We now switch on the hybridization between the metal $3d$ orbitals and the valence and conduction-band states. Hybridization between the ligand p orbitals and the metal d orbitals is included via the usual one-electron mixing matrix element T.[5,6] Here, $(pd\sigma)/(pd\pi) = -2.2$ (Refs. 5 and 6) reflecting the anisotropic hybridization strengths of the O $2p$ orbitals with the metal e_g and t_{2g} orbitals, with $T_\sigma = \sqrt{3}(pd\sigma)$ and $T_\pi = 2(pd\pi)$ for a cluster in an octahedral coordination.

An effective coupling parameter for describing the interaction strength between the central cluster d orbitals and the conduction band, T^*, is introduced analogous to the transfer integral T. In the case of scenario 2, T^* is simply proportional to the overlap between the metal $3d$ and $4sp$ orbitals. T^* is more difficult to define for scenario 1, however, where it describes the ease with which an electron can hop from one d site to another. Intersite hopping will be mediated by the intervening ligand orbitals, and so the magnitude of T^* will also reflect the strength of the intracluster hybridization determined by Δ and T. Charge transfer between d-

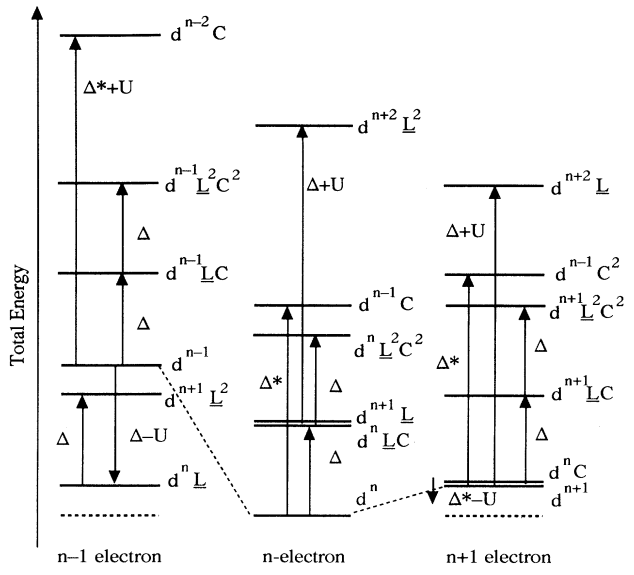

FIG. 1. Schematic many-electron total-energy diagram for the unhybridized ground state for scenario 1, as described in the text, for the neutral (n electron), electron-addition ($n+1$ electron), and the electron-removal ($n-1$ electron) states.

electron sites via the ligand orbitals will be more likely in highly covalent compounds, where the ligand p orbitals and the metal d orbitals are strongly mixed. Thus, T^* is expected to be significant for covalent compounds where Δ is small, and go to zero for more ionic compounds where Δ is larger. T^* is left as an effective parameter in the fitting procedure, reflecting the various interaction strengths required to transfer an electron into the conduction band.

The off-diagonal mixing matrix elements can be defined as

$$\langle d_\mu | H | L_\mu \rangle = T \ , \tag{12}$$

where $T = T_\sigma$ if μ indicates the $3z^2-r^2$ or x^2-y^2 orbitals and $T = T_\pi$ if μ indicates the xy, yz, or zx orbitals, and L_μ and d_μ are a ligand electron and a d electron with the same orbital symmetry, and

$$\langle d_\mu | H | C_\mu \rangle = T^* \ , \tag{13}$$

where C_μ and d_μ are a conduction-band electron and a d electron with the same orbital symmetry. Only states where an electron of the correct symmetry has been transferred either from the ligand orbitals to the TM site or from the TM site to the conduction band will have a nonzero overlap. As each spin and orbital state is considered individually, the degeneracy will be accounted for simply by the number of configurations. Any configuration dependence[22] in the transfer integrals has been neglected. The eigenfunctions for the ground state are found by diagonalization of the Hamiltonian matrix.

The configurations in the ground state for scenario 1 can be displayed diagrammatically as in Fig. 2. The left-hand most configuration is the lowest-energy ionic d^n state, with configurations increasing in energy by the addition of U (vertical axis) as extra electrons or holes are added, or by the addition of the band-gap energy $\Delta+\Delta^*-U$ (horizontal axis) as electrons are effectively transferred from the valence band to the conduction band. Hybridization between the configurations is indicated by arrows, with an upwards pointing arrow referring to Eq. (12), while a downwards pointing arrow refers to Eq. (13). Each arrow indicates a possible charge-transfer process. It can be seen that the configurations on the central horizontal line of the diagram will have a rela-

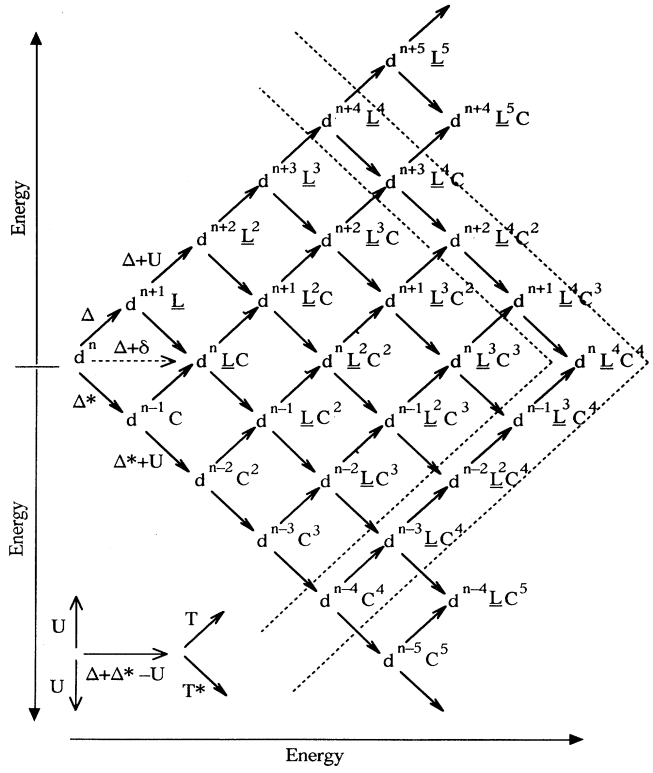

FIG. 2. Schematic configuration energy digram for the configurations in the ground state for scenario 1, as described in the text. Hybridization between configurations is indicated by arrows, with an upwards pointing arrow referring to T, while a downwards pointing arrow refers to T^*. Each arrow indicates a possible charge-transfer process. The left-hand most configuration is the lowest-energy ionic d^n state, with configurations increasing in energy by addition of U (vertical axis) as extra electrons or holes are added, and by addition to the band-gap energy $\Delta+\Delta^*-U$ (horizontal axis) as electrons are effectively transferred from the valence band to the conduction band. Dashed lines indicate the truncation of the basis set after six and eight charge-transfer processes.

tively lower energy than those above or below them and, therefore, will have a relatively larger weight in the ground state. In previous cluster models, only the upper left-hand most set of configurations was considered (d^n, $d^{n+1}\underline{L}$, $d^{n+2}\underline{L}^2$, etc.), while in the present model, we have a number of similar sets of configurations, where one or more electrons have been transferred to the conduction band. As the configurations towards the top and bottom of the diagram will be relatively higher in energy compared to the center, we can limit the scale of the calculation to a tractable size by truncating the basis set as indicated in the diagram. For a d^8 compound, this means that considering up to six charge-transfer processes gives us a total of 548 configurations.

In the unhybridized ground state of scenario 1, the configurations $d^{n+1}\underline{L}$ and $d^n\underline{L}C$ should be degenerate at energy Δ, as both states describe the transfer of an electron from a ligand orbital to a d-electron site. However, when the hybridization is switched on, as no direct overlap is considered between the d^n state and the $d^n\underline{L}C$ state (this is a two step process), the degeneracy is removed. To restore this degeneracy in the hybridized ground state, we must add an additional energy to those of the $d^n\underline{L}C$, $d^n\underline{L}^2C^2$, etc. states to account for the hybridization between the ligand orbitals and the orbitals of the neighboring d-electron sites, which cannot be directly incorporated into the single-impurity model. This effective energy is labeled δ and can be determined approximately by diagonalization of the Hamiltonian for a given set of parameters. The band gap in the hybridized ground state is then given by $\Delta+\delta$. δ is also added to these configurations in the final state.

The XPS final state will differ from the ground state by the attraction between the photoionization core hole and the $3d$ electron, Q. The core-hole interaction will tend to pull down the $3d$ levels where an extra electron is present at the TM site and push up the levels where an extra hole is present (Q is positive). Figure 2 can be altered to reflect the final state by subtracting Q from the configuration energies in the top half of the diagram and adding Q to those in the bottom half, and the final-state diagonal matrix elements are modified accordingly. We have neglected the exchange interaction between the core hole and the d electrons and assumed $U/Q \approx 0.83$ as before.[6] After finding the eigenfunctions of the final-state matrix, the XPS spectrum is calculated within the sudden approximation the usual way.[6]

Within this model, we have retained the same parameters Δ, U, and T_σ from previous models[6] to describe the intracluster metal-ligand interactions. Interactions between the TM impurity site and the conduction band are described by the parameters Δ^*, T^* and in the case of scenario 1, δ. As both Δ^* and δ are exactly defined quantities, the only extra parameter to be fitted in reinterpreting the experimental spectrum is T^*. Setting T^* to zero removes the screening channel to the conduction-band states and returns us to the simple-cluster model result. By having a knowledge of the best fit values for the intracluster parameters, we can introduce a finite value of T^* to fit the extra structures found in the experimental spectrum.

III. RESULTS AND DISCUSSION

A. NiS

We now apply the above model to reinterpret the Ni $2p$ XPS core-level spectrum of NiS. The hexagonal NiAs form of NiS exhibits a first-order metal-nonmetal transition at $T_t \approx 260$ K (Ref. 14) and has been classified as a charge-transfer insulator below T_t from photoemission studies.[23] The metallic phase above T_t shows Pauli paramagnetism, while the p-type semiconducting phase below T_t shows antiferromagnetism.[14] Recent high-resolution photoemission studies have found a correlation-induced band gap opening below T_t,[24] although there are no detectable changes in the gross features of the valence-band ultraviolet photoemission spectroscopy spectrum[23] or the core-level XPS spectrum[25] across T_t.

The core-level Ni $2p$ spectrum of polycrystalline NiS (Ref. 7) was obtained at room temperature, as described in Ref. 6. The background subtraction procedure has been described elsewhere.[6] As can be seen in Fig. 3(a),

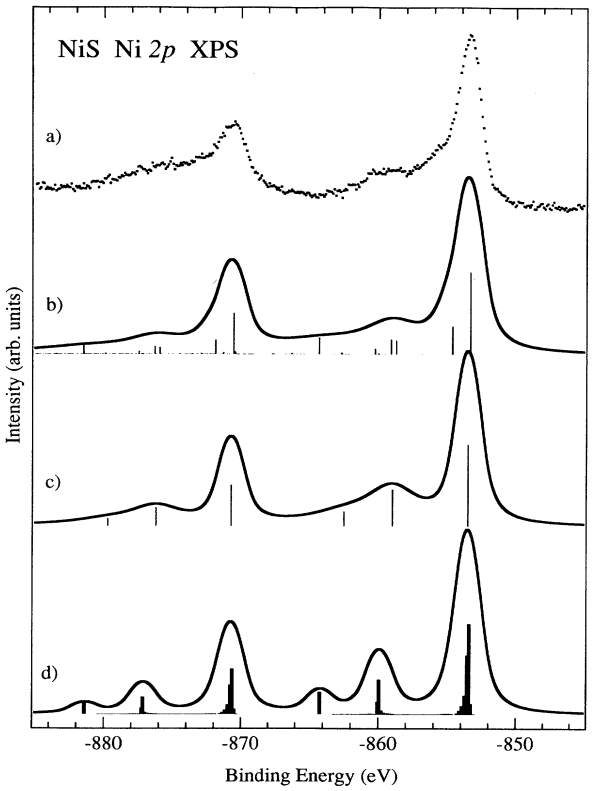

FIG. 3. Experimental (a) and calculated spectra for the Ni $2p$ core level of NiS within scenario 1 (see text), including calculations by a single-impurity cluster model, including charge-transfer effects to the conduction band (b); a single-impurity cluster model with intracluster interactions only (c); and an Anderson impurity model calculation (d). Intracluster parameters for all spectra are $\Delta=2.5$ eV, $U=5.5$ eV, and $T_\sigma=2.1$ eV, except for (d), where $T_\sigma=1.9$ eV. Conduction-band parameters for (b) are $\Delta^*=U$, $\delta=2.6$ eV, and $T^*=0.35$ eV. The intensity histogram spectrum is included for (d).

the main peak in the experimental spectrum shows a considerable asymmetry on the higher binding-energy side, with extra intensity appearing between the main peak and the satellite structure. This asymmetric line shape is also observed for $NiS_{1-x}Se_x$, NiSe, and NiTe,[7] as well as for $Ni_{1-x}M_xS$ (M=Co, Cr, V, Ti).[26] It is interesting to note that we find a similarly asymmetric line shape for the Ni $2p$ core level of the semiconducting intercalation compound $Ni_{0.33}TiS_2$ (Ref. 6), where the Ni cations are separated by alternating TiS_2 blocks. For this compound, the lowest-lying conduction band will comprise the empty Ti $3d$ orbitals instead of the empty Ni $3d$ orbitals.

Before introducing the interactions with the conduction band, we recalculate the simple-cluster model prediction for the core-level spectrum. This is obtained by setting the number of electrons transferred to the conduction band m in Eq. (4) to zero. We assume an idealized octahedral cluster consisting of a central Ni atom surrounded by S ligands. The ground-state wave function can be written as

$$\psi_g=\alpha|d^8\rangle+\beta|d^9\underline{L}\rangle+\gamma|d^{10}\underline{L}^2\rangle\ , \tag{14}$$

and the spectrum will have a three-peak structure. The calculated spectrum is compared with experiment in Fig. 3, and a best fit to the satellite intensity and energy separation from the main peak is obtained for the parameter values Δ=2.5 eV, U=5.5 eV, and T_σ=2.1 eV. These parameter values agree well with those found from CI studies of the valence band[23] and follow the general trends found for the late TM compounds.[6] We find a heavily mixed ground state consisting of 69% $|d^8\rangle$, 30% $|d^9\underline{L}\rangle$, and 1% $|d^{10}\underline{L}^2\rangle$, giving a d-electron number n_d of 8.32 or 0.32 holes transferred from the ligand sites. The main peak arises from the $|\underline{c}d^9\underline{L}\rangle$ final state, while the largest satellite is due to the $|\underline{c}d^{10}\underline{L}^2\rangle$ final state. An energy-dependent Lorentzian lifetime broadening[27] is included to simulate the core-hole d-electron multiplet splitting, and any additional splitting due to the off-diagonal d-d Coulomb exchange interactions neglected in the Hamiltonian. A Gaussian broadening is also included to simulate the instrumental broadening. As can be seen from Fig. 3(c), although we can correctly model the satellite position and intensity, it is impossible to reproduce the large asymmetry of the main peak using only this three-peak structure.

Retaining the same intracluster parameters Δ, U, and T_σ, we now introduce the interaction between the TM site and the conduction band. For our calculations, we have truncated our basis set after six charge-transfer processes in the manner shown in Fig. 2, meaning we only consider the intracluster configurations d^8, $d^9\underline{L}$, $d^{10}\underline{L}^2$, and the conduction-band screened configurations d^7C, $d^8\underline{L}C$, $d^9\underline{L}^2C$, $d^{10}\underline{L}^3C$, d^6C^2, $d^7\underline{L}C^2$, $d^8\underline{L}^2C^2$, $d^9\underline{L}^3C^2$, d^5C^3, $d^6\underline{L}C^3$, $d^7\underline{L}^2C^3$, and $d^8\underline{L}^3C^3$. We first consider scenario 1 as described in Sec. II, where $\Delta^*=U$. The hybridization correction term δ is calculated by setting T^* to zero and diagonalizing the Hamiltonian matrix for the above values of Δ and T to find the energy required to make the hybridized $d^9\underline{L}$ and $d^8\underline{L}C$ states degenerate. For these parameters, we find δ equal to 2.6 eV. This value simply reflects the hybridization splitting between the $|d^8\rangle$ and $|d^9\underline{L}\rangle$ states. We now switch on the charge-transfer channel to the conduction band by varying T^* to obtain a best fit to the room-temperature experimental data. The result for T^*=0.35 eV is shown in Fig. 3(b), where it is compared to the experimental data and the simple-cluster model result found above. The important features of this calculation are the extra intensity on the higher binding-energy side of the main peak, and the appearance of additional satellite structures at higher energies. We are able to reproduce the asymmetry of the main peak, while keeping the correct satellite to main peak ratio, which cannot be achieved using the three-peak structure of the simple-cluster model.

The various final-state components of the line spectra shown in Fig. 3(b) are displayed in more detail in Fig. 4, where we have grouped the components into sets with approximately ascending order of energy. While the main features in the spectrum still predominantly arise from intracluster interactions, considerable spectral weight also arises from states with an electron transferred to the conduction band. These include features at $\approx$2 and $\approx$11 eV from the main peak, mainly due to $|\underline{c}d^9\underline{L}^2C\rangle$ and $|\underline{c}d^{10}\underline{L}^3C\rangle$ final states, and an additional structure in the satellite region arising from $|\underline{c}d^8\underline{L}^2C^2\rangle$ and $|\underline{c}d^9\underline{L}^3C^2\rangle$

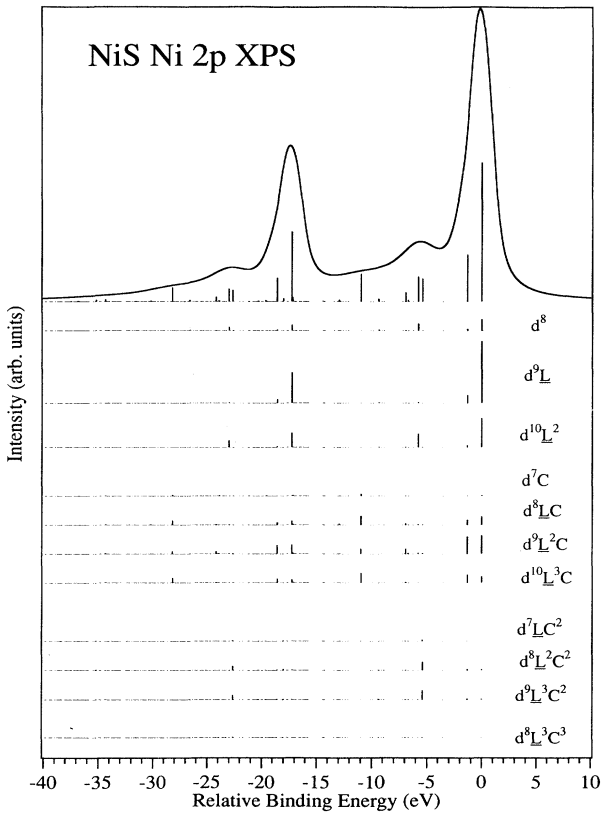

FIG. 4. Final-state components for the line spectrum displayed in Fig. 3(b). Components have been grouped into sets of approximately increasing energy.

final states. Although the total satellite intensity is largely unchanged, it is now spread out over a larger energy range.

The ground state is heavily mixed with most weight being distributed among the set of configurations with one electron transferred to the conduction band. These weights are listed in Table I, along with the calculation parameters. Charge-transfer states such as $d^8\underline{L}C$, $d^8\underline{L}^2C^2$, etc. will leave the total d-electron number effectively unchanged at the TM sites as in scenario 1, the electrons transferred to the conduction band reenter the TM orbitals again. Thus, if we consider that states such as $d^9\underline{L}$, $d^9\underline{L}^2C$, $d^9\underline{L}^3C^2$, etc., will all have effectively one electron transferred from the ligand site to the TM site, Table I gives us a total of 0.30 holes at the ligand sites, as for the simple-cluster model above. It should be noted that the intracluster interactions still dominate the ground state and NiS is described as a charge-transfer insulator within the model.

Figure 5 shows the effect of varying T^* on the spectrum. If T^* is large, weight is shifted out to the conduction-band screened states in the ground state, and the satellite intensity is weak and spread out over a large energy range. As T^* becomes smaller, the conduction-band screened states and the intracluster states become more evenly mixed, yielding strong satellite structures. As T^* goes to zero, the additional satellite structures arising from these states are reduced in intensity until we return to the simple-cluster model result.

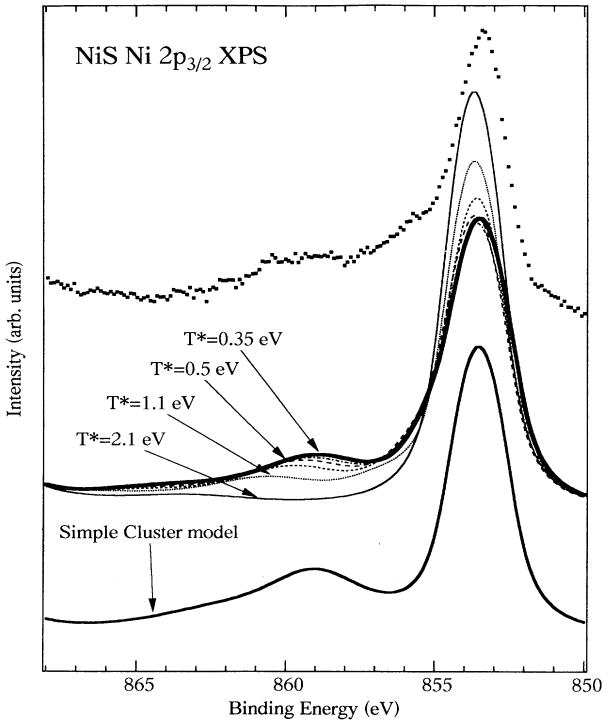

FIG. 5. Ni $2p_{3/2}$ spectra for NiS obtained by varying T^*. The result for $T^*=0.35$ eV is shown by a thick line. Also shown is the simple single-cluster model result and the experimental spectrum (dots). Other parameters are as for Fig. 3(b).

TABLE I. Parameter values used in the calculations for NiS [Fig. 3(b)] and NiO [Fig. 8(b)] (in eV), and the resulting weights for the configurations in the ground state. The basis set was truncated after six charge-transfer processes.

Parameter/ Configuration	NiS	NiO
Δ	2.5	4.5
U	5.5	7.5
T_σ	2.1	2.25
Δ^*	5.5	7.5
T^*	0.35	0.10
δ	2.6	0.7
d^8	0.20	0.49
$d^9\underline{L}$	0.07	0.13
$d^{10}\underline{L}^2$	0.01	
d^7C	0.10	0.07
$d^8\underline{L}C$	0.28	0.21
$d^9\underline{L}^2C$	0.14	0.08
$d^{10}\underline{L}^3C$	0.01	
d^6C^2	0.01	
$d^7\underline{L}C^2$	0.08	0.01
$d^8\underline{L}^2C^2$	0.09	0.01
$d^9\underline{L}^3C^2$	0.03	
d^5C^3		
$d^6\underline{L}C^3$		
$d^7\underline{L}^2C^3$	0.01	
$d^8\underline{L}^3C^3$		

It is interesting to compare the result obtained by the present model with that found from Anderson impurity model calculations. One could speculate that the asymmetric line shape is simply a consequence of the bandlike nature of the S $3p$ band and so should be reproduced using a standard impurity model calculation. The Anderson impurity model prediction for the Ni $2p$ spectrum for $\Delta=2.5$ eV, $U=5.5$ eV, $T_\sigma=1.9$ eV, and $W=3$ eV is displayed in Fig. 3(d), where W is the ligand bandwidth which was divided into 20 discrete states for the calculation. In this calculation, we have used a triangular e_g-projected ligand $3p$ density of states (DOS). Here, we have used a Lorentzian lifetime broadening of 0.6 eV and a Gaussian broadening of 1.2 eV to mimic instrumental effects. It is clear that although there is some small asymmetry on the high binding-energy side of the main peak, band effects alone cannot account for the intensity seen in the NiS spectrum. This calculation is similar to that by Zaanen, Westra, and Sawatzky[2] using intracluster parameter values very close to those above ($\Delta=2.6$ eV, $U=5.0$ eV, $T_\sigma=2.0$ eV, $U/Q=0.7$), with a 3-eV-wide semielliptical e_g-projected ligand $2p$ DOS. The asymmetry of the main peak may even be overestimated in these calculations as a more realistic picture of the e_g-projected S $3p$ DOS calculated using the LDA+U method by Anisimov, Zaaner, and Anderson[28] shows a very narrow partial DOS with a width of less than 1 eV. Therefore, we suggest that the asymmetric line shape of

NiS is not a consequence of the ligand bandwidth.

We can also compare the present model to the original model of Kotani and Toyozawa[29] for XPS core-level spectra. In this early model, the XPS satellite arises from an unscreened bound state and the main line is due to states where the core hole is screened. Here, the ground state is formed by filling the bound state and the lowest-lying Bloch states in the presence of the core hole until the Fermi level. The asymmetric line shape is due to the excitation of electron-hole pairs in the final state, where electrons can be excited into a continuum of empty Bloch states, which forms the conduction band. The situation is analogous to the present model, except that we now have a narrow bandwidth for the valence and conduction bands. In the present model, the main peak and satellite structures still arise from the intracluster final states, due to the strong core-hole potential. However, states where electrons have been excited into the conduction band will provide extra satellite structures in the spectrum, leading to an asymmetric main peak line shape.

We can also calculate the result predicted for scenario 2, where the conduction band is the Ni $4sp$ level by setting $\Delta^* = U + 5$ eV $= 10.5$ eV, as shown in Fig. 6. The line spectrum displayed in the figure is for the $T^* = 0.5$ eV spectrum. Although the satellite structure spreads out for large values of T^* as before, the conduction-band screened states are high in energy, and no new structures appear in the spectrum for smaller T^*. In fact, the best-fit result for this scenario is for $T^* = 0$. In other words, the current model provides no improvements over earlier models in this case.

In the previous calculations for scenario 1, we have applied the symmetry restriction that only the $e_g\uparrow$ orbitals could mix with the conduction-band screened states. For an idealized antiferromagnetically ordered cubic lattice where the metal-ligand-metal bonds are all 180°, such as in a perovskite oxide, only electrons of $e_g\uparrow$ character can be transferred to the unoccupied metal $3d$ orbitals of the neighboring d sites. For NiS, however, the hexagonal NiAs structure allows the Ni atoms to be situated much closer to each other with a metal-ligand-metal bond angle of less than 180°, leading to the possibility of a nonzero overlap between the occupied $t_{2g}\uparrow$ and $t_{2g}\downarrow$ orbitals and the unoccupied orbitals on neighboring sites. We can investigate this structural effect by setting $T^* t_{2g} = \alpha T^* e_g$, where $0 \le \alpha \le 1$, as shown in Fig. 7. Although there is some increase in intensity of the satellite structure, due to the conduction-band screened states, lifting the symmetry restriction for transfer to the conduction band has little effect on the overall shape of the spectrum in this case.

Finally, we discuss the convergence of the calculation with the size of the basis set. By keeping Δ^*, δ, and the

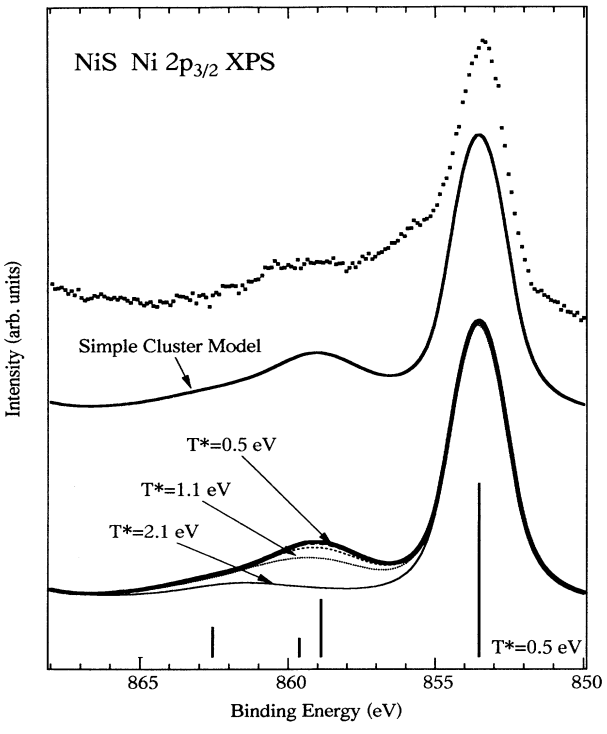

FIG. 6. Experimental (dots) and calculated spectra for the Ni $2p$ core level of NiS within scenario 2 (see text), obtained by varying T^*. The line spectrum is for $T^* = 0.5$ eV, which is shown by a thick line. Here, $\Delta^* = 10.5$ eV, $U = 5.5$ eV, and $T_\sigma = 2.1$ eV. No asymmetry is found for the main peak within this scenario.

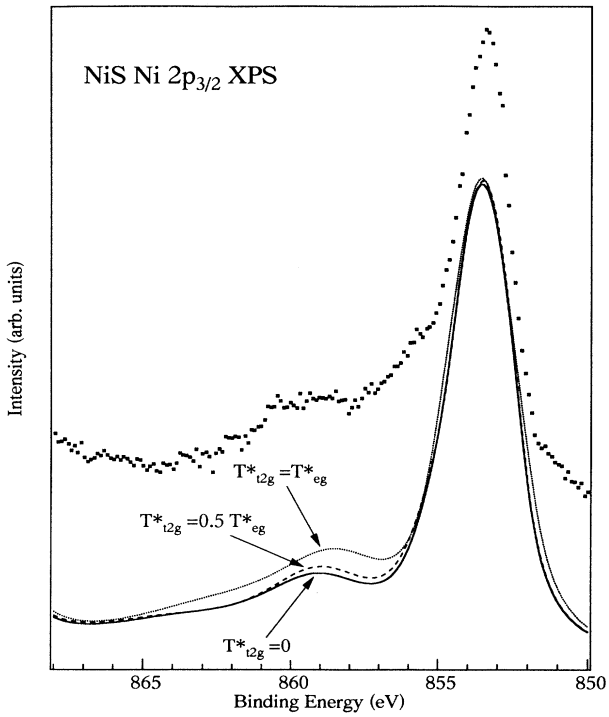

FIG. 7. Experimental (dots) and calculated spectra for the Ni $2p$ core level of NiS within scenario 1 obtained by lifting the symmetry restriction on charge transfer to the conduction band. Little change is seen in the line shape as we allow more t_{2g} electrons to enter the conduction band.

intracluster parameters constant, we can find the best-fit value of T^* for the calculated spectrum as the basis set size is increased up to eight charge-transfer processes. (Computational difficulties limit the size of the calculation to eight processes.) Although we find that T^* must be made smaller as the basis size is increased to reproduce the experimental spectrum, the sixth-order and eight-order results are sufficiently similar to suggest that the value of T^* is rapidly converging to a finite value. We also find that considering only up to fourth-order processes provides an insufficient basis set to yield any new information over the standard cluster model.

B. NiO

In order to ascertain whether our model can simulate the results obtained by a multiple-impurity approach, we calculate the Ni $2p$ spectrum of NiO. The lower panel of Fig. 8 shows the spectrum for a simple-cluster model without the conduction-band screened states compared to the experimental spectrum taken from Ref. 6. This result yields best-fit intracluster parameters of $\Delta=4.5$ eV, $U=7.5$ eV, and $T_\sigma=2.25$ eV, which are in accordance with those obtained in earlier studies.[6] Similar broadening procedures to those for NiS have been used for this spectrum. We now recalculate the spectrum within scenario 1, with $\Delta^*=U$ and $\delta=0.7$ eV, and vary T^* to obtain a best fit to experiment. Here, we use a basis set truncated after six charge-transfer processes. The result for $T^*=0.1$ eV is shown in the middle panel of Fig. 8, while the effect of varying T^* is illustrated in Fig. 9. As can be seen from the figures, a single-impurity model fails to reproduce the doubly peaked structure of the main peak. Although some new features are seen in the calculated spectrum at ≈ 1 eV and ≈ 12 eV from the main peak, the 1-eV feature is too weak to reproduce the double peak. As found for NiS, a larger T^* reduces the intensity of the satellite structures. Reducing T^* increases the satellite intensity to that of the experimental spectrum, but only weak intensity appears on the high binding-energy side of the main peak. As T^* goes to zero, the new satellite features in the spectrum disappear and we return to the simple-cluster model result. In fact, the best-fit result for NiO may be the simple-cluster model result with $T^*=0$.

The character of the satellite structures can be seen in more detail in Fig. 10, where the line spectrum of Fig. 8(b) is deconvoluted in the same manner as for Fig. 4. For a small value of T^*, the intracluster interactions dominate and there is very little mixing between the intracluster states and the conduction-band screened states. The main features in the spectrum have the same charac-

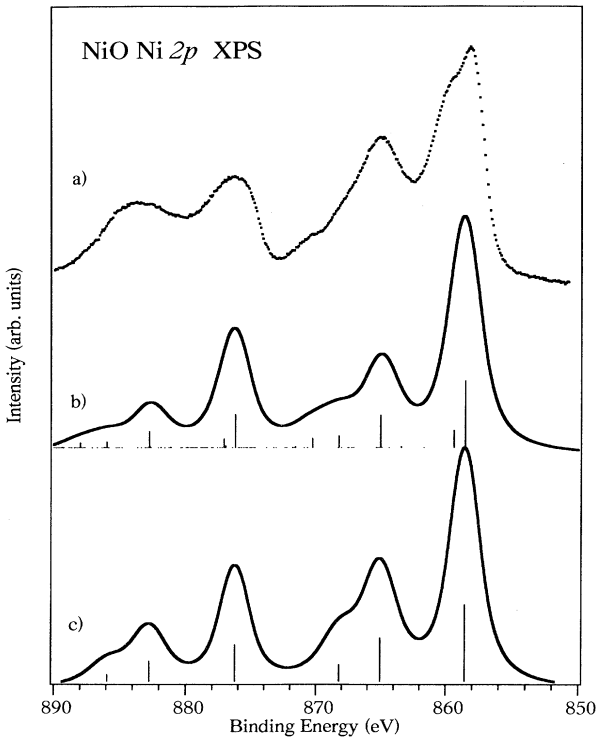

FIG. 8. Experimental (a) and calculated spectra for the Ni $2p$ core level of NiO within scenario 1 (see text), including calculations by a single-impurity cluster model including charge-transfer effects to the conduction band (b); and a single-impurity cluster model with intracluster interactions only (c). Intracluster parameters for both spectra are $\Delta=4.5$ eV, $U=7.5$ eV, and $T_\sigma=2.25$ eV. Conduction-band parameters for (b) are $\Delta^*=U$, $\delta=0.7$ eV, and $T^*=0.10$ eV. The experimental spectrum is taken from Ref. 6.

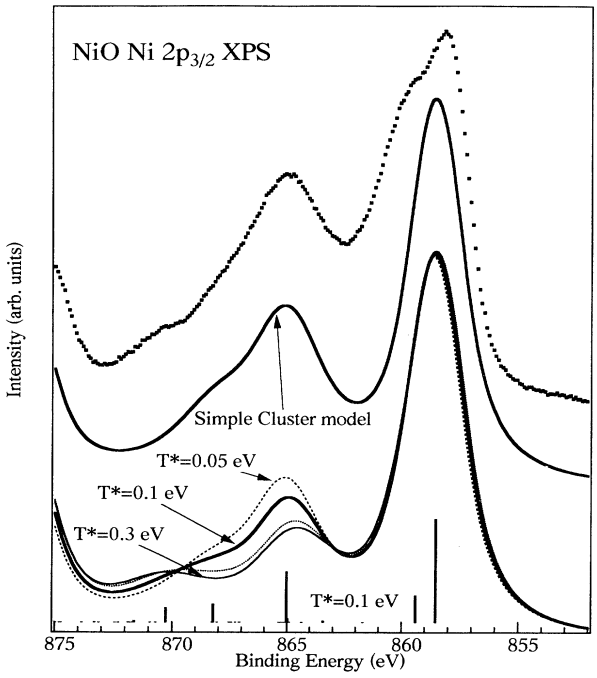

FIG. 9. Ni $2p_{3/2}$ spectra for NiO obtained by varying T^*. The line spectrum is for $T^*=0.10$ eV, which is shown by a thickened line. Also shown is the simple single-cluster model result and the experimental spectrum (dots). Other parameters are the same as for Fig. 9(b).

ter as for the simple-cluster result, with the new features arising from the lower-energy conduction-band screened states.

The failure of the present model to improve on the simple-cluster model result is related to the ionicity of NiO. As we go from NiS to NiO, both Δ and Δ^* increase by ≈ 2 eV, and the conduction-band screened states will be much higher in energy. The larger Δ for NiO means there will be less mixing between the ligand p orbitals and the Ni d orbitals, making it less feasible for hopping to occur between the d-electron sites. Thus, for more ionic compounds, screening by the conduction band becomes less important and the present model provides no new information on the ground-state electronic structure.

The reason why a multiple-impurity model predicts a double peak structure and a single-impurity model does not, can be explained in the following. In a multiple-impurity model, where we consider an impurity unit consisting of more than one TM ion, the double peak structure of the main peak for NiO (Refs. 8 and 9) results from energetically different screening channels in the final state, due to the presence of neighboring clusters. Here, the main peak becomes split into two components, where the lowest eigenstate of the spectrum is a state due to screening by a ligand electron from a neighboring cluster and has mainly $\underline{c}d^9;d^8\underline{L}$ character, where the notation indicates the configurations of the local TM ion cluster and a neighboring TM ion cluster.[8] This arises from the strong core-hole potential, and the stabilization energy gained by the ligand hole moving to the neighboring cluster.[8,9] The peak at higher binding energy corresponds to the original interpretation of the main peak within the single-impurity model and is due to local intracluster screening having mainly $\underline{c}d^9\underline{L};d^8$ character. Thus, the multiple impurity model prediction for the spectrum will have two main peaks, due to the almost degenerate nature of the screened final states. This situation is illustrated in the top panel of Fig. 11.

In a single-impurity model, where we only explicitly consider one d-electron site, this situation cannot be reproduced. In Fig. 11, we have compared the unhybridized ground and final states of the multiple- and single-impurity models. For the multiple-impurity model, the

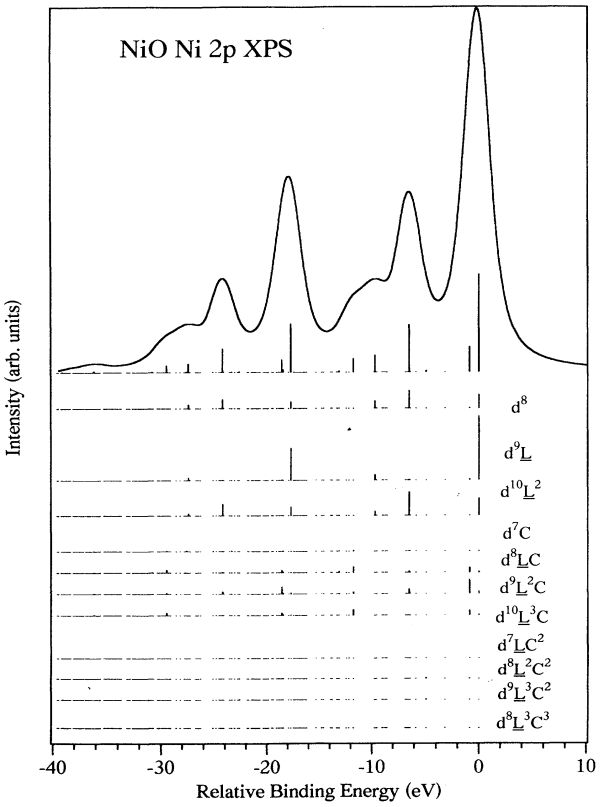

FIG. 10. Final-state components for the line spectrum displayed in Fig. 9(b). Components have been grouped into sets of approximately increasing energy.

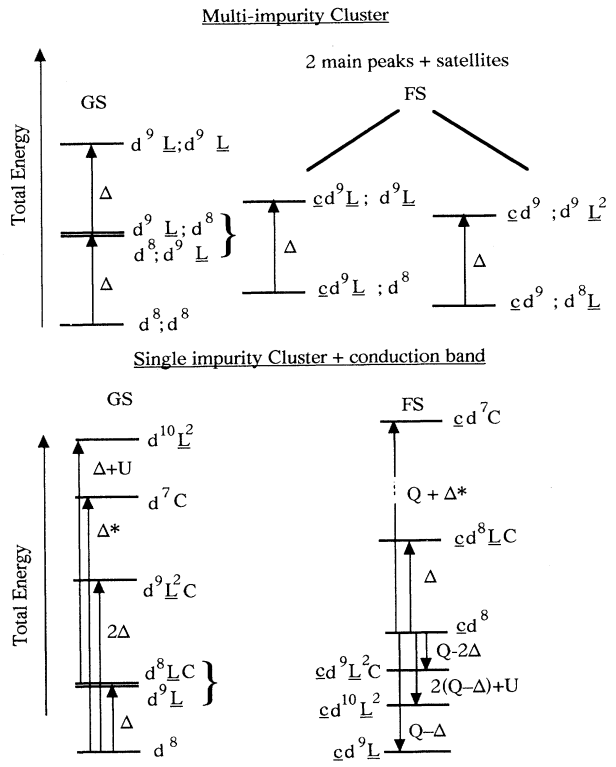

FIG. 11. Schematic energy-level diagram showing pertinent levels for the unhybridized ground and final states illustrating the differences between a multiple-impurity model consisting of two separate TM ion clusters and a single-impurity model including charge-transfer effects to the conduction band. For a multiple-impurity model, there are two almost degenerate final states representing different screening channels provided by the local and neighboring clusters. This leads to two main peaks close in energy in the spectrum. For the single-impurity model, although the conduction-band screened states provide new satellite structures, there will only be one main peak in the spectrum.

lowest-energy ground sate is $d^8;d^8$ and it costs Δ to add an electron to either cluster, to produce $d^8;d^9\underline{L}$ and $d^9\underline{L};d^8$ states. This is equivalent to the degeneracy of the $d^9\underline{L}$ and $d^8\underline{L}C$ levels in the single-impurity model. In the single-impurity final state, however, these levels are no longer almost degenerate, and we will always have only one main peak in the spectrum, although the conduction-band screened final states will provide a large number of new satellite structures. The strong core-hole potential will mean that the lowest-energy eigenstates of the spectrum will still be due to intracluster interactions, although they may be heavily mixed with those due to screening by the conduction-band electrons. Thus, the model is expected to provide a good starting point for the description of the ground state of compounds in which this screening is important, such as small gap semiconductors or highly covalent insulators where $T^*>0$. For more ionic compounds, screening by delocalized d electrons plays a lesser role and the best description by a single-cluster model may be the original localized approach with $T^*=0$.

IV. CONCLUSION

We have extended the single-impurity-cluster model to include the effects of charge transfer to the conduction band, and shown that these effects can have a considerable influence on the line shape of the $2p$ core-level spectra. The charge fluctuations between the TM site and the conduction band can be described by a few, well-defined parameters. We define an effective coupling parameter T^* to describe the interaction strength between the d-site orbitals and the conduction band. For a finite T^*, conduction-band screened states can mix heavily with the intracluster states in the ground state, causing the appearance of satellite structures in the spectra. As T^* goes to zero, these structures disappear and we return to the simple-cluster model result. For a scenario where the conduction band arises from the empty $3d$ orbitals on neighboring d sites, i.e., the upper Hubbard band, the model simulates part of the nonlocal screening channels from these d sites. In the case of NiS, the new model provides an improved interpretation of the Ni $2p$ core-level spectrum, where the asymmetric line shape of the main peak is reproduced, keeping the correct satellite to main peak ratio. For this small gap semiconducting (or metallic) compound, d-d screening via the conduction band is expected to play an important role in the electronic structure and T^* is expected to be significant. It should be noted, however, that the local intracluster interactions still dominate the electronic structure and the characters of the major features of the spectrum are still due to these states.

The model is less successful in simulating nonlocal screening effects in more ionic compounds, such as NiO, where the conduction-band screened states will be high in energy. Greater ionicity means the ligand p and metal d orbitals will be less heavily mixed, making hopping between d sites via the conduction band less feasible. In this compound, the best-fit result from the single-impurity model is for $T^*=0$, and the conduction-band screened states have little influence on the shape of the spectrum.

The present model may also be useful for investigating the electronic structures of light TM compounds, such as the Ti oxides or halides, where the large number of empty $3d$ states and strong metal-ligand covalency will inevitably lead to strong hybridization between neighboring clusters mediated by the intervening ligand orbitals. These compounds are considered to be typical Mott-Hubbard insulators with $U<\Delta$ and the influence of the empty metal states may become more important, with the largest contribution arising from the lower-lying upper Hubbard band.

In conclusion, we believe that the present model provides a good starting point for explaining in the metal $2p$ core-level line shapes of many small gap semiconducting or metallic compounds, such as the TM chalcogenides and the pyrite-type disulfide compounds MS_2 (M=Fe, Co, Ni). It also promises to be useful for the interpretation of the line shapes of other systems where metal-metal screening is important, such as for many U or Th compounds.

ACKNOWLEDGMENTS

The authors would like to thank Professor D. D. Sarma for many helpful discussions. We also thank Dr. H. Namatame for help in acquiring the data. This work was supported by a Grant-in-Aid from the Ministry of Education, Science and Culture, Japan. One of us (A.E.B.) gratefully acknowledges the support of the Japan Society for the Promotion of Science.

[1]O. Gunnarsson and K. Schönhammer, Phys. Rev. B **23**, 4315 (1983).
[2]J. Zaanen, C. Westra, and G. A. Sawatzky, Phys. Rev. B **33**, 8060 (1986).
[3]A. Fujimori and F. Minami, Phys. Rev. B **30**, 957 (1984).
[4]K. Okada and A. Kotani, J. Phys. Soc. Jpn. **61**, 4619 (1992).
[5]G. Lee and S.-J. Oh, Phys. Rev. B **43**, 14 674 (1991).
[6]A. E. Bocquet, T. Mizokawa, T. Saitoh, H. Namatame, and A. Fujimori, Phys. Rev. B **46**, 3771 (1992).
[7]M. Matoba, S. Anzai, and A. Fujimori, J. Phys. Soc. Jpn. **60**, 4230 (1991).
[8]M. A. van Veenendaal, H. Eskes, and G. A. Sawatzky, Phys. Rev. B **47**, 11 462 (1993).
[9]M. A. van Veenendaal and G. A. Sawatzky, Phys. Rev. Lett. **70**, 2459 (1993).
[10]M. A. van Veendaal, Ph.D. thesis, University of Groningen, 1994.
[11]S. Nimkar, Ph.D. thesis, Indian Institute of Science, 1993.
[12]M. A. van Veenendaal and G. A. Sawatzky, Phys. Rev. B **49**, 3473 (1994).
[13]M. A. van Veenendaal and G. A. Sawatzky, Phys. Rev. B **50**, 11 326 (1994).

[14]S. Anzai and K. Ozawa, J. Phys. Soc. Jpn. **24**, 271 (1968); J. T. Sparks and T. Komoto, Phys. Lett. **25A**, 398 (1967).
[15]K. Karlsson, O. Gunnarsson, and O. Jepsen, J. Phys. Condens. Matter **4**, 85 (1992).
[16]K. Karlsson, O. Gunnarsson, and O. Jepsen, J. Phys. Condens. Matter **4**, 2801 (1992).
[17]A. E. Bocquet, T. Saitoh, T. Mizokawa, and A. Fujimori, Solid State Commun. **83**, 11 (1992).
[18]A. Fujimori, A. E. Bocquet, T. Saitoh, and T. Mizokawa, J. Electron Spectrosc. Relat. Phenom. **62**, 141 (1993).
[19]A. Fujimori and T. Mizokawa, in *II-VI Semiconductor Compounds,* edited by M. Jian (World Scientific, Singapore, 1992), pp. 103–130.
[20]J. Kanamori, Prog. Theor. Phys. **30**, 275 (1963).
[21]J. Zaanen, G. A. Sawatzky, and J. W. Allen, J. Magn. Magn. Mater. **54-57**, 607 (1986).
[22]O. Gunnarsson and O. Jepson, Phys. Rev. B **38**, 3568 (1988).
[23]A. Fujimori, K. Terakura, M. Taniguchi, S. Ogawa, S. Suga, M. Matoba, and S. Anzai, Phys. Rev. B **37**, 3109 (1988).
[24]M. Nakamura, A. Sekiyama, H. Namatame, H. Kino, A. Fujimori, A. Misu, H. Ikoma, M. Matoba, and S. Anzai, Phys. Rev. Lett. **73**, 2891 (1994).
[25]A. Fujimori, M. Matoba, and S. Anzai (unpublished).
[26]T. Mamori, M. Matoba, A. Fujimori, and S. Anzai, J. Phys. Soc. Jpn. **61**, 433 (1992); M. Matoba, S. Anzai, and A. Fujimori, *ibid.* **63**, 1429 (1994).
[27]The Lorentzian full width at half maximum is taken such that $2\Gamma_n = 2\Gamma_0(1+\alpha\Delta E)$, where Γ_n is the lifetime broadening of the satellite peak, ΔE is the energy separation from the main peak, and α is a constant. In this case, $\Gamma_0 = 0.24$. For more detail see Ref. 6.
[28]V. I. Anisimov, J. Zaanen, and O. K. Anderson, Phys. Rev. B **44**, 943 (1991).
[29]A. Kotani and Y. Toyozawa, J. Phys. Soc. Jpn. **37**, 912 (1974).